ELSEVIER

Biophysical Chemistry 99 (2002) 209–228

Biophysical Chemistry

www.elsevier.com/locate/bpc

Effect of hydrophobic surfactant protein SP-C on binary phospholipid monolayers. Molecular machinery at the air/water interface

Peter Krüger[a,b], John E. Baatz[c], Richard A. Dluhy[a,*], Mathias Lösche[b]

[a]*Department of Chemistry, University of Georgia, Athens, GA 30602-2556, USA*
[b]*Institute of Experimental Physics I, University of Leipzig, Linnéstr. 5, D-04103 Leipzig, Germany*
[c]*Department of Pediatrics, Medical University of South Carolina, 165 Doughty Street, Charleston, SC 29425, USA*

Abstract

Fluorescent and modified dark-field microscopies were used to investigate the phase behavior of physiologically relevant lipid/protein monomolecular films containing surfactant protein C(SP-C). Synthetic human SP-C(1-34) was labeled at its N-terminus using the fluorescent probe 6-(((4(4,4-difluoro-5-(2-thienyl)-4-bora-3a,4a-diaza-*s*-indacene-3-yl)phenoxy)acetyl)amino)hexanoic acid (BODIPY/TR-X). Using dual fluorescent labeling (lipid and protein) in the monolayers, we have correlated (at physiologically small concentrations of the protein) the lipid phase separation and protein distribution in situ. A comparison of the lipid and protein dye fluorescent micrographs indicates that SP-C(1-34) is preferentially associated with the disordered lipid phase. Three concepts arise from our results. (1) The presence of SP-C alone does not result in the complete dissolution of condensed phase domains in a fashion that we have previously reported for the entire hydrophobic surfactant protein (SP-B/C) fraction (Biophys. J. 77 (1999) 903). Rather, the use of relatively high amounts (~10 wt.%) of the labeled SP-C protein is needed to reproduce the fluorescence monolayer morphology previously observed for small concentrations (~1 wt.%) of the natural SP-B/C mixture. (2) Scattered light, dark-field microscopy performed using grazing angle laser illumination reveals the presence of surface-associated, three-dimensional (3D) structures of micrometer-sized dimensions when the labeled BODIPY/TR-X:SP-C(1-34) protein is included in the monolayer, as previously observed with the naturally isolated SP-B/C mixture. The 3D structures are associated exclusively with the presence of the SP-C protein in disordered monolayer phases. (3) To explain these results, we have derived a molecular model accounting for the structure and physico-chemical properties of the SP-C protein in terms of its energetics. The molecular events involved in the SP-

Abbreviations: 2D, 3D, two-, three-dimensional; (A)RDS, (acute) respiratory distress syndrome; A/W, air–water; ATR, attenuated total reflectance; DPPC, 1,2-dipalmitoyl-*sn*-glycero-3-phosphocholine; DPPG, 1,2-dipalmitoyl-*sn*-glycero-3-phosphoglycerol; BODIPY-PC, 2-(4,4-difluoro-5,7-dimethyl-4-bora-3a,4a-diaza-*s*-indacene-3-dodecanoyl)-1-palmitoyl-*sn*-glycero-3-phosphatidylcholine; BODIPY/TR-X, 6-(((4(4,4-difluoro-5-(2-thienyl)-4-bora-3a,4a-diaza-*s*-indacene-3-yl)phenoxy)acetyl)amino)hexanoic acid; BODIPY/TR-X:SP-C(1-34), SP-C(1-34) labeled at the N-terminus with BODIPY/TR-X; Hepes, *N*-(2-hydroxyethyl)piperizine-*N*′-(2-ethanesulfonic acid); LE, LC, liquid expanded, liquid condensed monolayer phase; PBS, pulsating bubble surfactometry; SP-B/C, hydrophobic protein fraction isolated from pulmonary surfactant composed of surfactant proteins B and/or C; SP-C(1-34), synthetic human SP-C; TFA, trifluoroacetic acid.

*Corresponding author. Tel.: +1-706-542-1950; fax: +1-706-542-9454.
E-mail address: dluhy@chem.uga.edu (R.A. Dluhy).

0301-4622/02/$ - see front matter
PII: S0301-4622(02)00184-9

C-mediated production of the 3D surface particles are explained using the analogy of a simple molecular machine, namely a loaded spring. This interpretation is supported by an energetic analysis that suggests the major factor contributing to the formation of the 3D particles is the energy liberated by re-expansion of the surrounding phospholipid film into the area vacated by the SP-C protein as it re-orients away from the surface.

Keywords: Pulmonary surfactant; Lipid–protein interactions; Lipid monolayer phases; Fluorescence; Scattered light microscopy

1. Introduction

To facilitate breathing, it is required that surface tension at the air–alveolar interface in the mammalian lung be reduced to near zero from the normal value of 72 mN/m at the air–water (A/W) interface [1]. In vivo, surface tension is regulated by pulmonary surfactant, a lipid–protein complex that may be isolated from lung lavage [2]. Deficiency of this material causes respiratory distress syndrome in premature infants [3], and has also been implicated in the acute version of respiratory distress syndrome, which is often trauma-related [4]. The gross composition of typical surfactant isolates is 90% lipid and 10% protein by weight, with the main lipid classes being the phosphocholines (PCs) and phosphoglycerols (PGs) [5]. Pulmonary surfactant isolates contain approximately 50% by weight of the biologically uncommon, fully saturated phospholipid 1,2-dipalmitoyl-*sn*-glycero-3-phosphocholine (DPPC) [6]. Progress in isolating surfactant components [7] has advanced to the point where biophysical approaches may be utilized to understand how the interaction between components leads to surfactant function. These biophysical approaches are also necessary for the rational design of exogenous surfactants for therapeutic purposes [8].

An important area of recent surfactant research has been to address the influence of the major hydrophobic surfactant proteins on the physical structure of phospholipid surfactant models. The protein fraction of pulmonary surfactant contains at least four major components, designated SP-A, SP-B, SP-C and SP-D [9,10]. Neither SP-A nor SP-D are primarily responsible for the surface-active characteristics of native lung surfactant [11]. However, the other two hydrophobic surfactant proteins, namely SP-B, and SP-C, have been implicated in surfactant surface activity and have been extensively biochemically characterized. Both SP-B and SP-C are of low molecular weight, are hydrophobic in character, and are membrane-associated. They have been shown to enhance the rate of phospholipid adsorption from vesicles [12–14]. Several studies have also indicated that model phospholipid mixtures reconstituted with these hydrophobic surfactant proteins can mimic the surface activity of natural pulmonary surfactant [15,16]. For these reasons, the SP-B and SP-C surfactant proteins have received increasing attention in biophysical studies.

Optical microscopy has proven especially useful in the study of surfactant monolayer model systems. For example, the mixing behavior of binary lipid systems that mimic surfactant lipid compositions has been studied using fluorescence microscopy [17,18]. The effects of the hydrophobic surfactant proteins SP-B and SP-C, or fragments of these proteins, on lipid domain morphology have also more recently been studied using fluorescence, near-field and scanning force methods [19–24]. These imaging studies have begun to map out the role of these hydrophobic proteins in the surfactant-associated functions of spreading and readsorption.

In a previous paper [25], we used fluorescent and dark-field microscopy at the air/water interface to investigate a ternary model system composed of the phosphocholine and phosphoglycerol surfactant lipids that contained the entire hydrophobic surfactant protein fraction (both SP-B and SP-C proteins) at physiologically relevant concentrations (~1 wt.%). We showed that a SP-B/C mixture induced the formation of a new phase in the surface monolayer of intrinsically lower order than the liquid condensed phase. Applying a modified dark-field microscopy method we were able to detect three-dimensional (3D), micrometer-sized, surface-associated exclusions from the monolayer. These exclusion bodies formed only with

the SP-B/C proteins and provided direct optical evidence for the predicted squeeze out of surfactant monolayer material upon increasing monolayer surface pressure.

In this work, we focus on the effect of synthetic SP-C alone—in physiologically relevant concentrations—on the monolayer structure of phosphocholine and phosphoglycerol binary lipid mixtures. The sensitivity of fluorescence microscopy, in combination with the specificity of dark-field microscopy for visualizing particle structures, enables us to trace topological changes brought about by protein concentrations of $\sim$1 wt.% with respect to the lipid and allows us to explore the mechanism of formation of the observed 3D exclusion bodies. The synthesis of a fluorescently labeled SP-C protein permits a correlation of lipid phase separation and protein distribution in situ. A molecular scenario accounting for the molecular structure and physico-chemical properties of the SP-C protein is derived and discussed in terms of its energetics.

2. Materials and methods

2.1. Synthetic materials

The synthetic phospholipids DPPC and 1,2-dipalmitoyl-*sn*-glycero-3-phosphoglycerol (DPPG) were from Sigma (Deisenhofen, Germany). They were specified as better than 99% pure, and used as supplied. Chain-labeled PC (2-(4,4-difluoro-5,7-dimethyl-4-bora-3a,4a-diaza-*s*-indacene-3-dodecanoyl)-1-palmitoyl-*sn*-glycero-3-PC, BODIPY-PC) was from Molecular Probes (Leiden, The Netherlands). Chloroform from Merck (Darmstadt, Germany) and methanol from Sigma were of *pro analysis* (p.a.) grade.

2.2. Synthesis of labeled and unlabeled SP-C(1-34)

Synthetic human SP-C(1-34) was synthesized using Fmoc chemistry [26]. The synthetic protein was labeled at the N-terminus using the fluorescent amine-reactive probe BODIPY/TR-X SE (6-(((4-(4,4-difluoro-5-(2-thienyl)-4-bora-3a,4a-diaza-*s*-indacene-3-yl)phenoxy)acetyl)amino)hexanoic acid succinimidylester; Molecular Probes, Eugene, OR). The unlabeled protein was first solubilized with trifluoroacetic acid (TFA), followed by slow addition of HPLC grade acetonitrile (ACN, Sigma Chemical Co., St. Louis, MO), and then slow drop-wise addition of HPLC grade methanol (MeOH, Sigma Chemical Co., St. Louis, MO) with constant stirring. The final solution consisted of SP-C protein in 2:1 MeOH/ACN + 0.1% TFA. pH was adjusted to 7.4 using 1.0 M NaH_2PO_4/Na_2HPO_4 buffer, pH 7.4. An appropriate volume of BODIPY/TR-X in DMSO was added to the SP-C solution to provide a 6$\times$ molar excess in fluorescent adduct. The mixture was incubated in an amber reaction vial at 25 °C for 3 h with continuous stirring. Hydroxylamine (1.5 M) was used to stop the reaction. Purification of the SP-C(1-34) labeled at the N-terminus with BODIPY/TR-X (BODIPY/TR-X:SP-C(1-34)) was achieved by C8 liquid chromatography. The C8 column was pre-equilibrated and eluted with 1:1 $CHCl_3$:MeOH with 0.5% 0.1 M HCl as described elsewhere [27]. The degree of labeling (label to protein ratio of 1.1:1.0) and final protein concentration were determined according to the protocol of the manufacturer (Molecular Probes). Previous studies have demonstrated the similarities in surface activities of labeled SP-C with unlabeled native SP-C using this method of derivatization [28].

2.3. Characterization of labeled and unlabeled SP-C(1-34)

We have characterized the physical structure and surface activity properties of the synthetic SP-C(1-34) proteins using infrared spectroscopy and pulsating bubble surfactometry (PBS). IR spectra were obtained of SP-C(1-34) or BODIPY/TR-X:SP-C(1-34) as thin films cast from organic solution in the presence of a DPPC lipid matrix. Spectra were obtained using a Mattson (Madison, WI) RS-1 FT-IR spectrometer with liquid-N_2-cooled HgCdTe detector in the attenuated total reflectance (ATR) mode. A dried film of the lipid–protein mixture was prepared for IR analysis by placing an aliquot of the sample in organic solution onto a horizontal Ge ATR plate, where the solvent was allowed to evaporate. Spectra were acquired

at $4/cm^{-1}$ resolution with 512 scans and triangular apodization.

The overall surface tension lowering ability of the SP-C(1-34) and BODIPY/TR-X:SP-C(1-34) peptides on 7:1 DPPC:DPPG suspensions was measured using a pulsating bubble surfactometer (General Transco Inc, Largo, FL) [29]. Samples were prepared in a 20-mM Hepes (*N*-(2-hydroxyethyl)piperizine-*N*′-(2-ethanesulfonic acid) buffer, pH 6.9, with 120 mM NaCl. A small air bubble, communicating with ambient air, was formed in 40 μl of labeled or unlabeled SP-C(1-34)—lipid dispersion held in a plastic sample chamber. The bubble was then pulsated at 20 cycles/min between maximal and minimal radii of 0.55 and 0.4 mm, respectively, and the pressure drop across the A/W interface was measured with a precision pressure transducer. The surface tension at minimum bubble radius (minimum surface tension) was calculated as a function of time using the Laplace equation for a spherical interface [30]. The concentration of surfactant samples for bubble studies was uniform at 1.5 mg phospholipid/ml [31], with the unlabeled or labeled SP-C(1-34) peptide concentration at 2% (wt./wt.) with respect to total phospholipid. All bubble experiments were done at 37 ± 0.5 °C.

2.4. Surface chemistry and epi-fluorescence microscopy

Surface pressure–area (π–A) isotherm and microscopy measurements were performed at room temperature ($T \sim 20$ °C) on a Langmuir film balance of local design [25]. Water for the aqueous subphases was filtered (Millipore Milli-Q, Eschborn, Germany); its ionic strength was adjusted to 120 mM with NaCl (Fluka, Neu-Ulm, Germany, p.a.) and its pH to 6.5 with K_2HPO_4/KH_2PO_4 buffer. The buffer concentration did not exceed 1 mM. The fluorescence and grazing-angle illumination setup used to characterize molecular surface films has been described earlier [25]. Briefly, the BODIPY-PC or BODIPY/TR-X:SP-C(1-34) fluorescence is excited through an optical microscope (Axiotech Vario, Carl Zeiss, Jena, Germany) using a 50 W Hg lamp with excitation filters either in the 450–490 nm (lipid label) or the 515–555 nm (protein label) range. Emission was selected by using a 520 nm long-pass filter—transmitting both the lipid and protein label fluorescence light—or a band filter in the 515–555 nm region—transmitting exclusively the lipid label fluorescence. Emission from the protein label only was selected using a 590 nm long-pass filter. These optical filter band pass regions correspond to the components of the Carl Zeiss standard filter sets 9, 11 and 16. Scattered light microscopy was simultaneously performed with fluorescence microscopy using diode laser ($\lambda \sim 630$ nm) illumination at a shallow angle (measured to the interface), as described [25].

3. Results

In recent fluorescence microscopy work [25], we have observed the phase coexistence morphology of mixed lipid monolayers (DPPC:DPPG 7:1) in the regime within and above the first order phase transition observed in the isotherm, and have characterized the influence of a natural mixture of SP-B and SP-C on such textures at physiological concentrations (~ 1 wt.% total protein with respect to total phospholipid); see, e.g. figures 1 and 3 in Ref. [25]. In order to investigate the impact of the individual components of pulmonary surfactant, we report here on the influence of a synthetic analogue of SP-C, i.e. SP-C(1-34), on such mixed lipid monolayers.

3.1. Structure and activity of labeled and unlabeled SP-C(1-34)

We have obtained IR spectra of the labeled and unlabeled SP-C(1-34) to determine how fluorescent labeling of SP-C(1-34) affected the physical structure of the molecule. Mature, native SP-C consists of 35 amino acids and is an extremely hydrophobic, predominately α-helical protein of approximately 4.2 kDa with charged amino acids (K10 and R11) near its N-terminus. The NMR structure of SP-C in apolar solvent essentially describes the protein as a rigid rod in which only a few residues near the N-terminus (L1–P7) and the C-terminus itself are *not* helical [32].

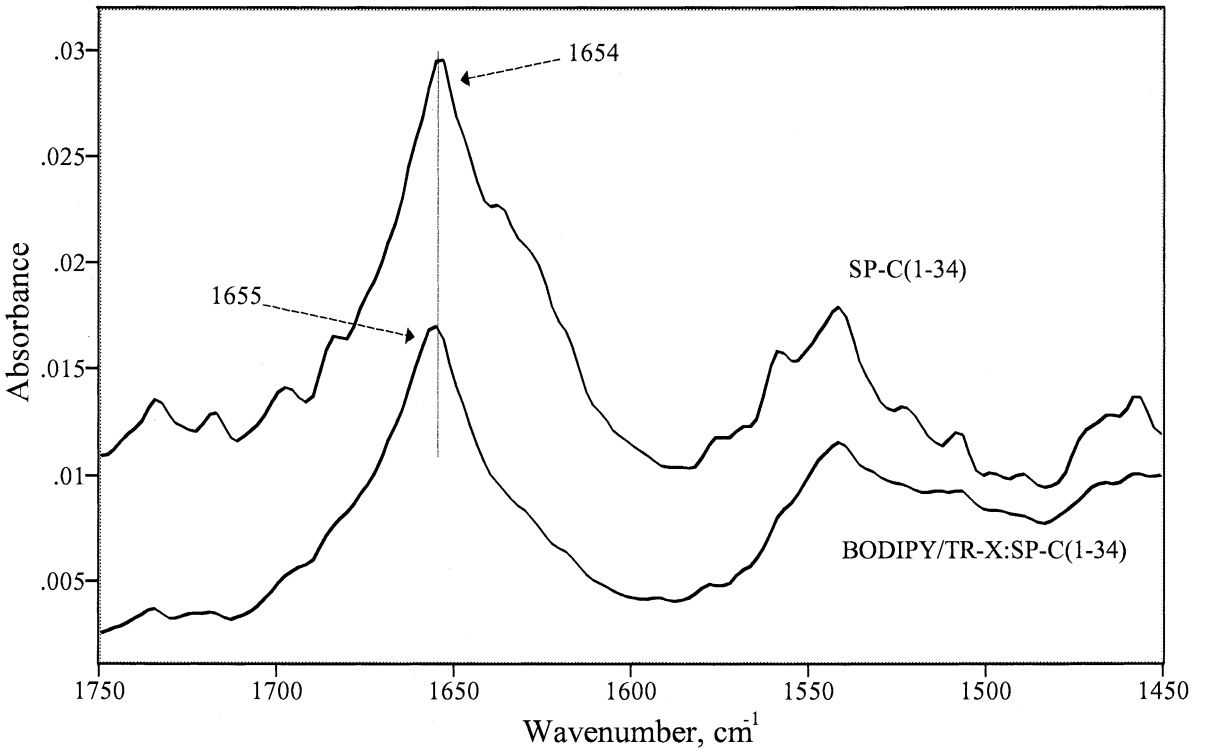

Fig. 1. Infrared spectra of the amide I and amide II regions (1750–1450/cm^{-1}) for synthetic SP-C analogues incorporated in DPPC vesicles. Upper trace is the unlabeled synthetic SP-C(1-34). Bottom trace is the fluorescently labeled BODIPY/TR-X:SP-C(1-34). In both cases, the infrared spectrum of DPPC vesicles was subtracted from the peptide/DPPC spectrum to yield the spectrum shown.

The IR spectra of the synthetic SP-C proteins shown in Fig. 1 were obtained as lipid–protein complexes. To obtain these IR spectra, the labeled and unlabeled proteins were co-solubilized in MeOH/$CHCl_3$ solution with the phospholipid DPPC at a protein concentration of 10 wt.% with respect to the lipid. The lipid–protein complex was then applied to the ATR plate and the organic solution was allowed to evaporate. The IR spectrum of DPPC was subtracted from the lipid–protein spectra, revealing the spectrum of the synthetic protein.

Fig. 1 presents the IR spectrum of the synthetic SP-C(1-34) analogue in the amide I and amide II regions between 1750 and 1450/cm^{-1} (upper trace). The most dominant peak in the spectrum is the amide I vibration at 1654/cm. Using well-established IR secondary structure—wavenumber correlations [33], this peak wavenumber value is associated with an α-helical secondary structure. The IR spectrum of the BODIPY/TR-X-labeled SP-C(1-34) protein is also presented in Fig. 1 (bottom trace). The amide I IR peak for the labeled protein is seen at 1655/cm^{-1}; the wavenumber, bandwidth and intensity of this peak are virtually identical to the amide I IR spectrum of the unlabeled SP-C(1-34) protein. Therefore, the synthetic fluorescent labeling of the SP-C(1-34) protein has not changed the fundamental α-helical secondary structure of SP-C(1-34), which is also characteristic of the native SP-C protein.

We have also investigated the surface activities of the synthetic SP-C(1-34) proteins using PBS. The principle behind PBS is that a decrease in measured surface tension is associated with the adsorption of the solute at the interface; any interfacial protein leading to a surface tension decrease is said to be ‘surface-active’. The surface

tension values obtained from the PBS experiments with either the labeled or unlabeled SP-C(1-34) proteins are presented in Table 1. These PBS measurements were made using lipid–protein dispersions containing labeled or unlabeled SP-C(1-34) in 7:1 DPPC:DPPG vesicles; surfactometry was used to ascertain how labeling of the SP-C(1-34) with BODIPY/TR-X affected the surface activity properties of the labeled protein relative to unlabeled protein. As indicated in Table 1, both SP-C(1-34) and BODIPY/TR-X:SP-C(1-34) slowly reduced surface tension over a 10-min period, reaching nearly identical surface tension values at the end of the period (26.4 and 24.3 mN/m, respectively).

These results are consistent with introduction of the label having no effect on surface activity of SP-C(1-34). Taken together with the ATR spectra of the two peptides, these two independent methods indicate that fluorescent labeling did not significantly change either the structural or surface-active properties of SP-C(1-34).

Table 1
Surface activity of labeled and unlabeled synthetic SP-C(1-34) as measured by PBS

Time (min)	Surface tension (mN/m)	
	SP-C(1-34)	BODIPY/TR-X:SP-C(1-34)
1	40.2 ± 0.5	35.0 ± 0.2
5	30.1 ± 0.7	26.4 ± 0.9
10	26.4 ± 0.9	24.3 ± 0.3

3.2. Binary lipid monolayers with unlabeled SP-C(1-34)

The results described in this section were obtained with low, physiologically relevant levels (2 wt.%) of synthetic SP-C(1-34) added to 7:1 DPPC:DPPG monolayers, i.e. DPPC:DPPG/SP-C(1-34). Images were obtained using the BODIPY-PC lipid fluorescent probe.

Fig. 2 shows the isotherm ($T \sim 20$ °C) and fluorescence micrographs of a DPPC:DPPG/SP-C(1-34) mixed lipid monolayer. The fluorescence images occur at various pressures above the onset of the monolayer phase transition in which the contrast between the ordered lipid phase (dark areas) and disordered lipid phase (bright areas) has been visualized by admixture of 0.2 mol.% (with respect to total lipid) BODIPY-PC. As with pure lipid monolayers, ordered domains from shortly after the onset of the phase transition (Fig. 2, 7.0 mN/m image)—as indicated by the sharp kink in the isotherm (cf. Fig. 2).

In contrast to our observations with a SP-B/C mixture [25], there is no dissolution of the ordered lipid domains observed in the course of the phase transition. Rather, the domain boundaries persist and stay well defined even at high surface pressure; see Fig. 2 micrographs at 15 and 25 mN/m. The influence of the unlabeled SP-C(1-34) protein is revealed by the fact that the boundary shapes of the ordered domains deviate somewhat from that observed in the pure lipid system as well as a rather inhomogeneous label distribution in the fluid lipid phase. The influence of SP-C(1-34) at the interface is not as clear at these protein concentrations as was the influence of the hydrophobic SP-B/C mixture [25]. At high surface pressure, the SP-C(1-34)-affected domain textures appear to crumble into small areas rather than dissolving continuously, as observed in both the pure lipid monolayers and lipid monolayers with the natural SP-B/C mixture [25], albeit at different characteristic surface pressures.

In agreement with our previous work, we have found that inspection of the isotherms for 1% protein in 7:1 DPPC:DPPG at pH's between 6.2 and 7.0 reveals negligible differences. In fact, at any pH above the pK_a of the phosphoglycerol headgroup (~ 5.6), not only are the isotherms indistinguishable, but the fluorescent images obtained for this system are identical. This confirms that the ionization state of the PG headgroup controls the lipid—SP-C(1-34) interactions, as we have previously discussed [25].

In comparison with the SP-B/C mixture, SP-C(1-34) alone does not result in dissolving of the ordered lipid domains in the characteristic fashion we have previously reported [25]. The condensed phase domains are somewhat smaller at high π, but even there, visual contrast of the edges of the

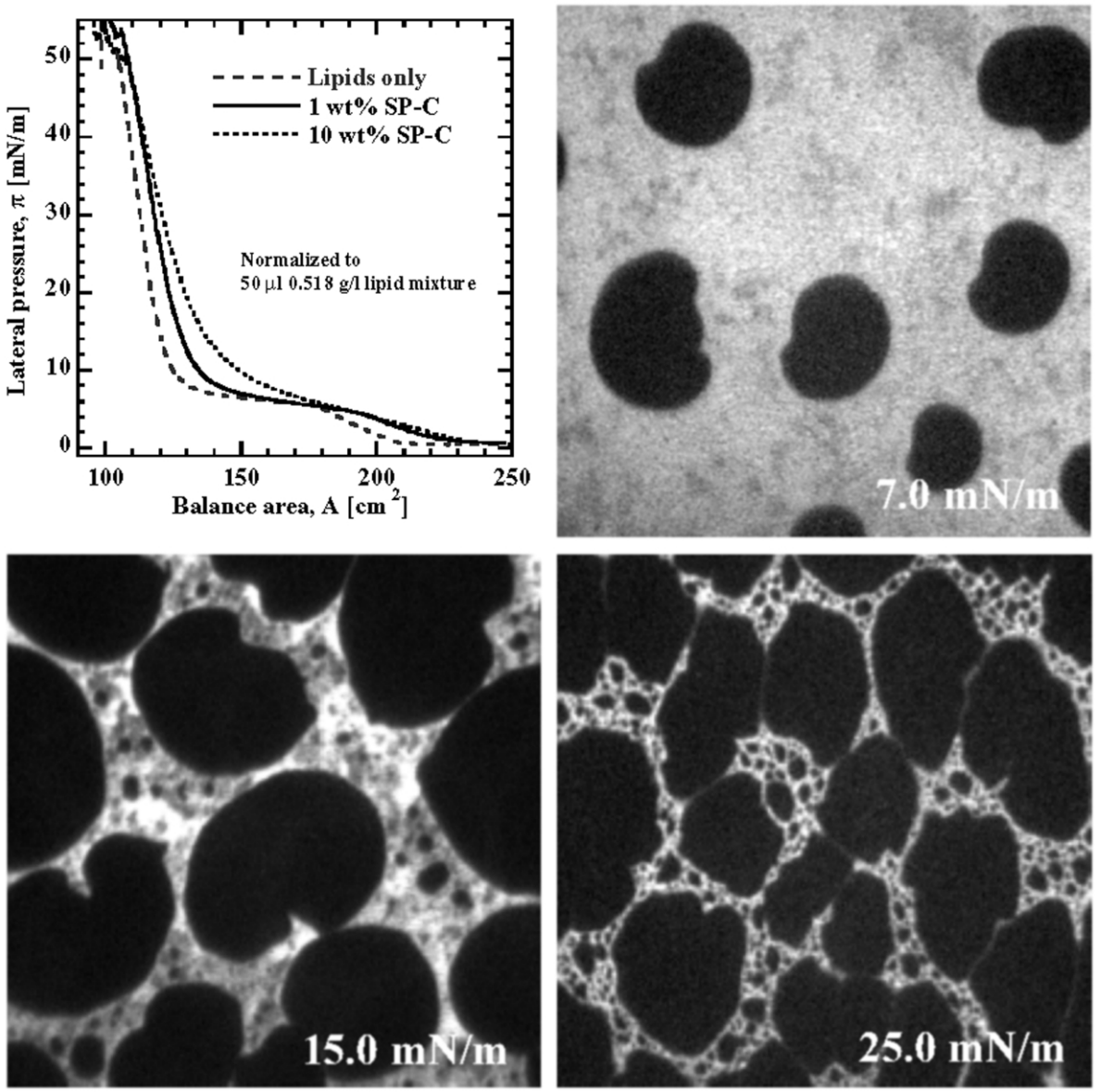

Fig. 2. Room temperature ($T=20\pm1$ °C) isotherms of a 7:1 DPPC:DPPG/SP-C(1-34) monolayer with various amounts of the protein as indicated and representative fluorescence micrographs (150×150 μm^2; 0.2 mol.% BODIPY-PC with respect to total lipid) of this lipid mixture with 2 wt.% of (unlabeled) SP-C(1-34) protein. The flat portion in the isotherms indicate the liquid expanded–liquid condensed (LE–LC) phase transition [57].

solid phase domains is maintained. The major consequence of introducing SP-C(1-34) into the lipid monolayer is the formation of smaller, fragmented condensed phase domains at high π that are interdispersed among the larger domains.

3.3. Binary lipid monolayers with BODIPY/TR-X labeled SP-C(1-34)

In order to address the question of the distribution of SP-C within the monolayer with respect to

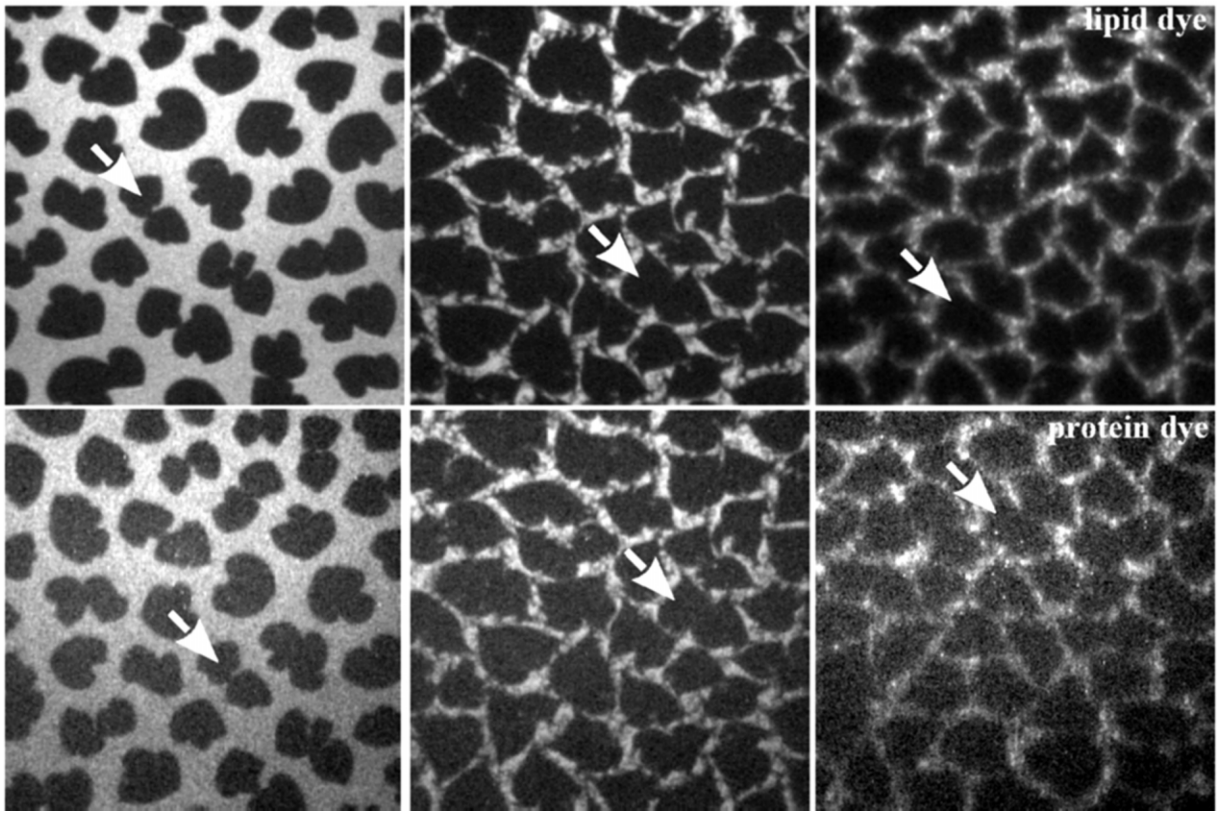

Fig. 3. Dual label fluorescence microscopy results for a 7:1 DPPC:DPPG/BODIPY/TR-X:SP-C(1-34) (1 wt.%) monolayer with 0.2 mol.% BODIPY-PC at various surface pressures as indicated. Image sizes are 150×150 μm^2. *Upper panels:* BODIPY-PC emission; *lower panels:* BODIPY/TR-X emission. Arrows indicated monolayer features that correspond to each other in the lipid and protein dye images. Temperature is 20 ± 1 °C.

the coexisting lipid phases, we have performed dual-label experiments using both BODIPY-PC and BODIPY/TR-X:SP-C(1-34) in mixed DPPC:DPPG surface films. Results in this section were obtained with low levels (1 wt.%) of the protein label BODIPY/TR-X:SP-C(1-34) added to a 7:1 (mol:mol) mixture of DPPC:DPPG. In addition, the lipid label BODIPY-PC was added to the 7:1 DPPC:DPPG/TR-X:SP-C(1-34) mixture at 0.2 mol.% relative to the total lipid content. Fluorescence emission from the lipid and protein labels was obtained independently using the filter settings described in Section 2. The lipid and protein images shown here were consecutively obtained within approximately 1 min of each other by changing the position of the filter cube in the Zeiss Axiotech microscope, followed by image acquisition.

Fig. 3 illustrates three pairs of fluorescence micrographs that visualize similar areas in the monolayer films at various pressures in the emitted light of the either the lipid or the protein label. Fluorescent images obtained of lipid domain distribution in the presence of BODIPY/TR-X:SP-C(1-34) differ from those observed for the non-labeled SP-C(1-34). The main differences appear in the distribution of the condensed phases and the presence of the intermediate 'third phase' [25]. Compression of the DPPC:DPPG/TR-X:SP-C(1-34) system forms condensed phases through the phase transition region, as also observed in the DPPC:DPPG/SP-C monolayer (Fig. 2). However,

these condensed phase domains maintain a more jagged and irregular appearance, as opposed to the more circular and normal, 'kidney-shaped' domains [34] in the DPPC:DPPG system. Note that the images shown in Fig. 2 were acquired using 1 wt.% SP-C(1-34) while the images in Fig. 3 were acquired using 2 wt.% of the BODIPY/TR-X:SP-C(1-34). We have observed no differences in the fluorescent images acquired when using physiological amounts (1–2 wt.%) of the SP-C(1-34) protein.

At $\pi \sim 14$ mN/m, the condensed phase domains in the DPPC:DPPG/TR-X:SP-C(1-34) system begin to dissolve along their periphery, forming a network structure resembling that which we have previously observed in the DPPC:DPPG/SP-B/C system. This solid phase dissolution progresses as the surface pressure increases, however, the dissolution of the solid domains does not go to completion, as in the DPPC:DPPG/SP-B/C system. Even at relatively high surface pressure (30 mN/m), a substantial fraction of the monolayer exists in the condensed phase. Similarly, the network structure of the 'third phase' that is formed in the DPPC:DPPG/TR-X:SP-C(1-34) system beyond $\pi \sim 14$ mN/m is not nearly as extensive as that previously seen in the DPPC:DPPG:SP-B/C system. Although the dissolution of the solid phase domains begins at approximately the same surface pressure in the two systems, it appears to be essentially completed by ~ 22 mN/m with BODIPY/TR-X:SP-C(1-34), thus demonstrating that the SP-C protein alone, apart from SP-B, has a much weaker propensity for disrupting the condensed phase.

Two major conclusions result from these experiments: (a) SP-C(1-34) is preferentially associated with the disordered lipid phase, as most clearly revealed from a comparison of the lipid and protein dye micrographs in Fig. 3, and (b) a dissolution of the ordered lipid domains at high surface pressure—as reported earlier for the natural SP-B/C mixture—is observed in the system only if fluorescently labeled SP-C(1-34) is used instead of the unlabeled synthetic protein (compare the 30 mN/m micrograph in Fig. 3 with the 25 mN/m micrograph in Fig. 2). In contrast with the complete dissolution of the ordered lipid phase upon interaction with the natural SP-B/C mixture—see figure 3 in [25]—BODIPY/TR-X:SP-C(1-34) does not completely dissolve the condensed phase domains, but rather remains primarily in the fluid phase. This results in large fractions of condensed phase lipid that are retained in the monolayer even at high surface pressures.

As used in our fluorescence studies of surfactant proteins, the word 'dissolution' refers to the transformation of condensed phase domains having well-defined, sharp interfaces into domains in which the domain interface becomes fragmented and forms branches that emanate outward from the remaining condensed domain. These branches possess a fluorescent intensity (gray level) that is intermediate between that of a condensed and liquid phase. These branches are not uniformly distributed into the liquid phase, but rather form a new phase that grows at the expense of the solid and liquid phases. In certain cases, these branches so intermingle with one another and dominate the resulting images that it appears as if a network of these structures is formed. Presumably, because of the fluorescent gray level, the intrinsic order of this new phase is intermediate between that of a truly solid condensed phase and that of a fluid liquid phase. This new phase apparently is able to solubilize the lipophilic dye better than the solid condensed phase, but not as well as a fluid liquid phase, thus leading to the intermediate gray levels that we see in the micrographs. The predominance of these network structures having a fluorescent intensity intermediate between solid condensed and fluid liquid is consistent with a 'third phase'. The word 'dissolve' is used here in the sense that the effect of the protein is to solubilize the interfaces of the solid condensed phases, leading to the formation of this new network. This nomenclature is the same as what we employed in our previous fluorescent article on SP-B/C [25] and is retained here for clarity in comparison of the two studies.

3.4. Binary lipid monolayers with BODIPY/TR-X labeled SP-C(1-34) at high concentrations

Results in this section were obtained with ~ 10 wt.% of BODIPY/TR-X:SP-C(1-34) added to 7:1 DPPC:DPPG. BODIPY-PC was added to the 7:1

DPPC:DPPG/TR-X:SP-C(1-34) mixture at approximately 0.2 wt.%. The lipid and protein fluorescent images were recorded immediately after each other by switching between the respective filter sets. Hence, these images are indicative of both the lipid and protein phase distributions at the indicated surface pressure in the monolayer simultaneously (within ~1 min).

The fluorescence micrograph results obtained using ~10 wt.% of BODIPY/TR-X:SP-C(1-34) are shown in Fig. 4. Both the fluorescent lipid and protein fluorophores show essentially identical distributions within the monolayer at π values in the expanded region, as well as the phase transition region (up to ~25 mN/m). These results indicate that the BODIPY/TR-X:SP-C(1-34) protein resides in the fluid, disordered phase. Beyond 25 mN/m, the protein fluorescent images lose contrast. However, the lipid images from the BODIPY-PC may be observed at all surface pressures.

Lipid fluorescent images show that at 10 wt.%, the BODIPY/TR-X:SP-C(1-34) protein acts very much like the fully hydrophobic SP-B/C surfactant protein fraction did at 1 wt.% [25]. That is, dissolution of the condensed phase domains begins at ~17 mN/m and becomes progressively more prominent as π increases, unlike the case of the low concentration 1 wt.% DPPC:DPPG/TR-X:SP-C(1-34) system (see previous section), in which the dissolution was essentially completed at 22 mN/m. The 10 wt.% DPPC:DPPG/TR-X:SP-C(1-34) mixed monolayer approximates that of the 1 wt.% DPPC:DPPG/SP-B/C system especially well at higher π (>25 mN/m). In this case, the condensed phases are almost all dissolved, with only residual condensed phase remaining. In addition, the 'third phase', which is characterized by a fluorescence intensity intermediate between that of the solid and liquid state, and which has previously observed in the case of DPPC:DPPG/SP-B/C, is also prominently observed in these images. Just as in the DPPC:DPPG/SP-B/C system, the presence of 10 wt.% BODIPY/TR-X:SP-C(1-34) protein results in almost the entire area occupied by this phase that produces a fluorescent intensity intermediate between that of a solid and a liquid state.

3.5. Combined fluorescence with scattered light microscopy

Results in this section were obtained with ~10 wt.% of BODIPY/TR-X:SP-C(1-34) added to 7:1 DPPC:DPPG monolayers. BODIPY-PC was added to the 7:1 DPPC:DPPG mixture at approximately 0.2 wt.%. The lipid and protein fluorescent images, as well as the scattered light images, were obtained consecutively using the appropriate filter sets or by illuminating the surface with the laser. Hence, these images are indicative of both the lipid and protein phase distributions at the indicated surface pressure in the monolayer simultaneously (within ~2 min).

Consecutive images from fluorescence (lipid or protein), as well as scattered light microscopy, are presented in Fig. 5. At π>20 mN/m, they reveal excluded, surface-associated, 3D particles. This is illustrated for two surface pressure values above the main monolayer phase transition, π~26 and 55 mN/m. For each π, the first column shows lipid fluorescence distribution, the second column shows protein fluorescence distribution, and the third column shows scattered light results. The lipid and protein fluorescent images at 26.4 mN/m (top half of Fig. 5) reinforce the results described in the previous sections; that is, the lipid and protein fluorescence images are essentially identical, indicating that the protein is excluded from the condensed phases and resides primarily in the disordered phases.

Fig. 5 also illustrates the fact that protein clustering is occurring in this system. Evidence for this clustering comes from bright white spots in the fluorescence images taken with the 520 nm long-pass emission filter that transmits both the lipid label and protein label fluorescence. With the emission band-pass filter (515–555 nm) that passes the lipid label fluorescence only, these spots are not observed.

The observation of particles adhering to the monolayer is dependent on the presence of the TR-X labeled SP-C. Exclusion bodies are only observed in the current work in monolayers with BODIPY/TR-X:SP-C(1-34) (or, previously, in monolayers with the naturally occurring SP-B/C mixture) and are only observed in the fluid phase,

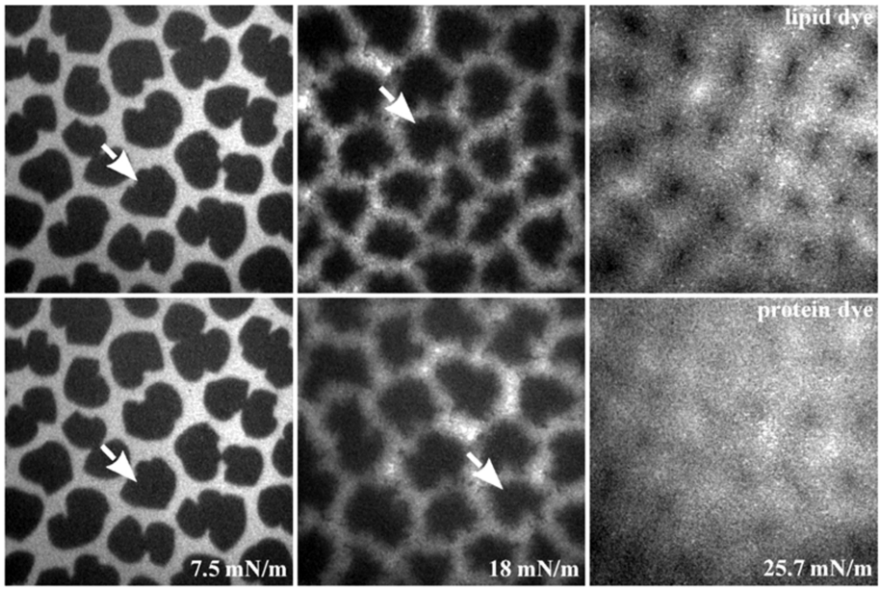

Fig. 4. Dual label fluorescence micrographs as in Fig. 2, but with 10 wt.% of the fluorescently labeled protein, BODIPY/TR-X:SP-C. Image sizes are 150×150 μm^2. Arrows indicated monolayer features that correspond to each other in the lipid and protein dye images. Temperature is 20 ± 1 °C.

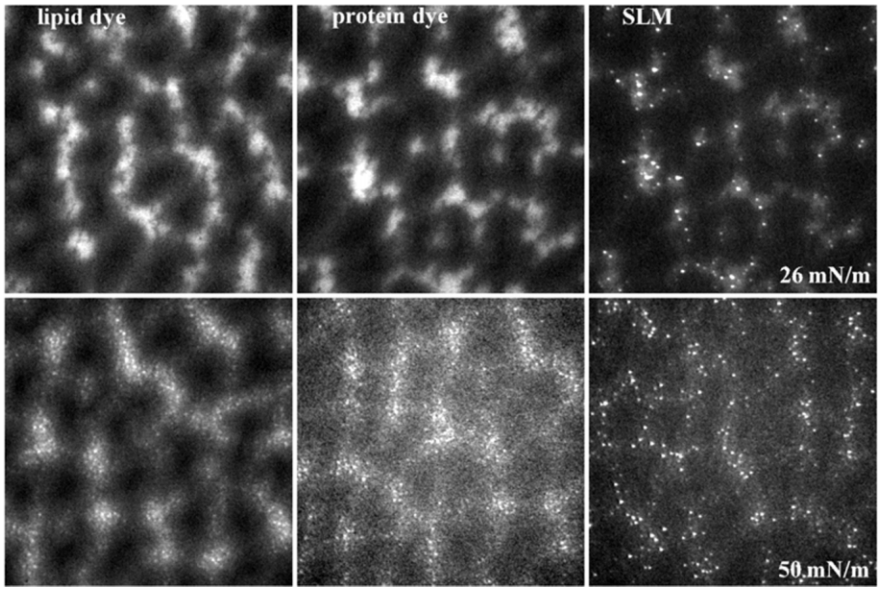

Fig. 5. Correspondence between fluorophore (BODIPY-PC, left, or BODIPY/TR-X, middle) distribution and the formation of surface-associated 3D particles (right) for a 7:1 DPPC:DPPG/BODIPY/TR-X:SP-C (10 wt.%) monolayer at two surface pressures above the LE–LC phase transition. Image sizes are 150×150 μm^2. Images at the same pressures have been recorded in short succession and show approximately the same areas within the monolayers. Temperature is 20 ± 1 °C.

where the SP-C is located, as indicated by the protein label fluorescence. As π is increased to 50 mN/m (lower half of Fig. 5), the fluorescence images from both lipid and protein are essentially identical. However, the number of bright spots visible using scattered light illumination has increased dramatically, indicating the abundance of surface-associated exclusion bodies. As before, this excluded material is associated exclusively with disordered monolayer phases.

4. Discussion

4.1. Comments on the use of physiologically relevant amounts of surfactant protein

A number of prior studies have addressed the biophysical roles played by both SP-B and SP-C in the function of pulmonary surfactant. In these studies, it has not been uncommon to study protein contents much higher than those encountered in vivo. The current work examined a range of protein contents, but with a focus on physiologically relevant levels (1–2 wt.%) in investigating interactions with lipids in the surface monolayer.

Over the years, several biophysical studies have examined the effects of physiologically relevant levels of surfactant proteins in lipid mixtures [19,20,35,36]. For example, Dluhy et al. [35] used IR spectroscopy to study molecular behavior in films of bovine lung surfactant containing endogenous ratios of protein and lipid components. Also, more recent investigations using near-field and scanning probe techniques to visualize transferred monolayer films used SP-B and SP-C concentrations of 2 wt.% [19,20].

Historically, however, biophysical studies have used relatively high surfactant protein concentrations, many of which use protein amounts far exceeding physiological levels. For example, IR studies of SP-B and SP-C in lipid monolayers at the A/W interface or in bulk phase vesicles have incorporated these proteins at weight percentage between 3 and 80% [37–39]. Also, optical microscopy studies of SP-C—containing monolayers, or of monolayers that contain synthetic proteins based on the truncated N-terminus of SP-B (i.e. SP-B_{1-25}), have used protein amounts that span a wide range between 2 and 28 wt.% [21–24,40,41]. Previous authors [37,42] found concentration-dependent results, and have stated that a precise determination of protein amounts may be critical for interpretation.

Of course, the use of non-physiological levels of exogenous protein in surfactant biophysical studies may be justified due to the nature of the experiment of the limitations of methodology. Nevertheless, high protein concentrations can lead to anomalous behavior such as protein aggregation and lipid–protein interactions driven by non-physiological energetics. Our prior optical microscopy data indicate a distinct difference in monolayer morphology upon addition of higher amounts of protein [25]. In addition, a recent IR study [43] has determined that maximum lipid perturbation occurs only at physiological protein levels. These concerns must be taken into consideration when trying to draw conclusions concerning physiological responses from model systems containing artificially high protein levels.

4.2. Relationship of this work to other studies of SP-C

Our scattered light microscopy results show that small 3D particles are formed during compression of mixed DPPC:DPPG monolayers containing either SP-B/C or BODIPY/TR-X:SP-C(1-34)—but not with unmodified SP-C(1-34). As argued in our recent work [25] and also seen here, particles are presumably located on top of the surface monolayers. This is indicated by the fact that one needs to adjust the focus slightly ($\sim$1 μm) above the monolayer for best visualization and by the fact that the intensity scattered from these particles ($\varnothing$ $<$1 μm) is very high. A large refractive index difference between particle and surrounding is likely, and the index difference between organic matter and air is larger than its difference to water.

Optical microscopy can help provide information concerning the molecular details of the surface layer reorganization. We have observed light scattering from 3D particles on lipid monolayers containing the natural SP-B/C mixture, but also from systems that contained only BODIPY/TR-X:SP-

C(1-34), i.e. without SP-B, but not with systems that contained the unmodified SP-C(1-34) as the only protein component. The general features of structure transformation reported in this work are quite similar to that in the SP-B/C system. From this we speculate that the exclusion particles are produced by a mechanism that depends critically on the presence of the rigid-rod-like molecule, SP-C, and that SP-B plays an auxiliary role in the process.

In previously published studies of pure recombinant, acylated SP-C monolayers, a phase transition has been reported [44] in the surface pressure range where we have detected the formation of a 'third phase'—or the dissolution of the ordered lipid phase—in fluorescence microscopy. This transition in pure SP-C monolayers was found associated with a thickness jump of the (average) surface layer thickness of about a factor of two, which was interpreted as a collective reorganization of the SP-C at the surface. More recently, a $\pi - A$ relation has been established for DPPC:DPPG/SP-C surface layers, that were similar in composition to the systems that have been studied in this laboratory, which shows a broad, non-equilibrium plateau at a surface pressure beyond 50 mN/m and a large hysteresis upon re-expansion [45]. Using ex situ methods, the SP-C dependent formation of membrane adherent particles has been demonstrated in the course of this non-equilibrium plateau [19,45,46], and a model for the formation of multibilayer phospholipid reservoirs, stabilized by SP-C, has been proposed [19,47]. It has also been established for transferred surfactant model surface layers that SP-C is associated with the disordered phase in mixed phospholipid/SP-C monolayers in a phase-separated state [19,48] and that SP-C is incorporated in the exclusion particles that adhere to the surface structure after transfer to solid substrates [19].

While these studies concentrated on the characteristics of the high-pressure non-equilibrium plateau, the properties of the model surface layers at low surface pressure—where we have reported the nucleation of membrane adherent particles [25]—have not been addressed. Therefore, the observations in our work relate to those previously published in that the small 3D particles detected by light scattering represent nucleation events for the formation of large-scale membrane adherent surfactant reservoirs, matured in the course of the high-pressure plateau to form extended multibilayer stacks as previously proposed.

The previous published optical microscopy studies of transferred SP-C monolayers that have observed 3D structures [19,47,48] have used human recombinant SP-C in their studies. These studies implicate SP-C in the formation of 3D structures at the A/W interface; however, direct comparison of the results from synthetic SP-C with human recombinant SP-C would be tentative. The results presented here make it possible to go one step further than previous studies by permitting the development of a mechanism and energetics necessary for SP-C—dependent reorganization of the surface structure.

4.3. Proposed mechanism of surface structure reorganization

As explained in the previous section, we are interested in the primary, molecular events that lead to the surface structure reorganization of the pulmonary system upon compression to high surface pressure. Putting the available pieces of information together, one may construct a model describing the effect of the SP-B/C system in catalyzing the first stage of structural reorganization of the pulmonary surfactant surface layer as a molecular machine which explains all the obtained results consistently. Within this model, SP-C plays a key role, acting as a hydrophobic rigid rod that may rotate around a hinge region, located at the flexible, hydrophilic C-terminus of the molecule, which serves to invert a few phospholipid molecules to form a locally confined bilayer structure, whereas SP-B attains an auxiliary role in the proposed molecular mechanism.

Key stages of the molecular events are schematically depicted in Fig. 6. At low surface pressure, the SP-C helix is oriented at a shallow angle from the interface with its N-terminus anchored at the A/W interface, as determined from FT-IR results [38]; the hydrophobic helix is thus immersed into the hydrocarbon chain layer of the surrounding phospholipid molecules. As suggested

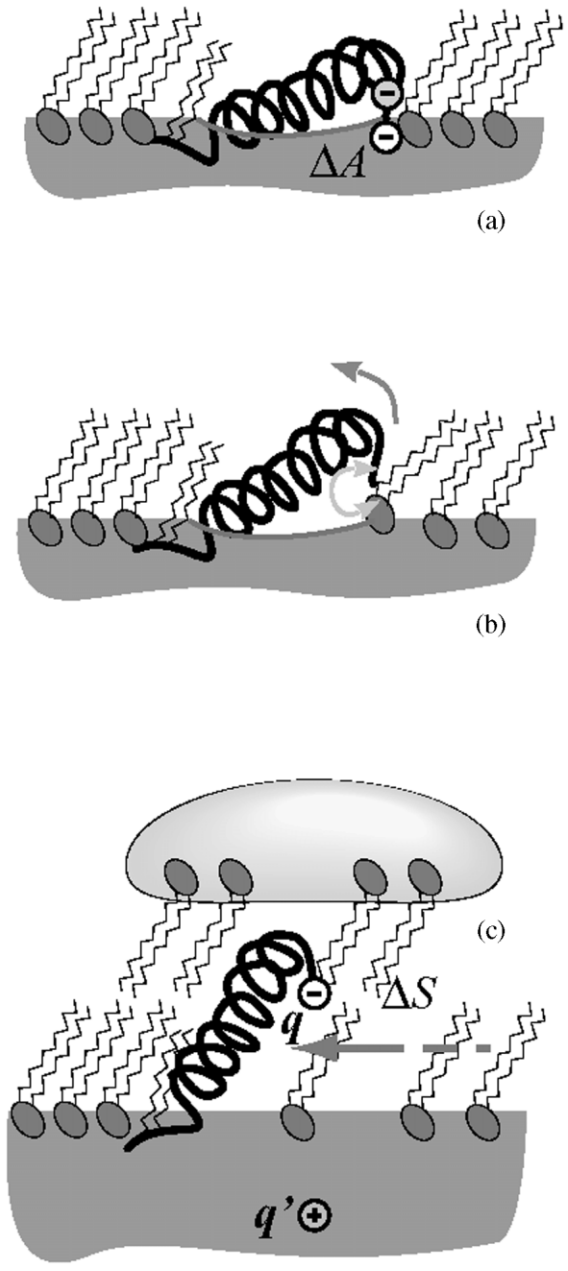

Fig. 6. Schematic representation of the molecular events leading to the formation of surface-associated microparticles that adhere to the monolayer. For details and an estimate of the energetic contributions to the entire process, see text.

by the pH dependence of the 3D particle formation upon compression [25], the anionic PG lipid component is preferentially associated with the protein, presumably with the positively charged N-terminus with $R2^+$ in its vicinity and $K11^+/R12^+$ near the N-terminal end of the hydrophobic helix. Both the cluster of charges near/at the N-terminus and the negatively charged C-terminus—by virtue of the terminal ~10 Å stretch of the protein chain that does not participate in helix formation [32]—are embedded into the aqueous subphase. The palmitoylation at adjacent cysteines in the N-terminal region prevents a deep penetration of the N-terminus into the subphase compartment and leads thus to the observed, flat orientation of the helix. As a result, a sizeable area of the hydrophobic helix is in contact with water molecules; such an energetically unfavorable conformation is, however, stabilized by hydrophobic contacts within the hydrocarbon layer and by charge–image charge *repulsion*. The latter occurs since the protein's charged C-terminus is embedded in the subphase, i.e. a high refractive index medium, which leads to the creation of an image charge across the boundary to the low refractive index hydrocarbon compartment. Since the index gradient from the real charge to the image charge is negative, the image charge bears *the same sign* as its parent real charge, which leads to repulsion between real charge and image charge; such repulsion may serve to lock the protein molecule into its orientation preferentially parallel to the interface the hydrophobic 'rigid rod' bears essential features of a potential spring.

Upon reduction of the area available to the surface film during compression, the overall energy of the systems rises continuously. While this rise in energy would not be sufficient to squeeze phospholipid molecules out of the surface monolayer individually or collectively, it is sufficient to overcome the (weak) electrostatic repulsion that locks the protein's C-terminus into its position at the hydrophilic/hydrophobic interface. As this happens, not only the helix axis is reoriented toward the interface normal, but also a number of lipid molecules, associated with the helix through hydrophobic contacts are lifted out of the monolayer surface film and inverted to form a local

bilayer structure—extending their hydrophilic headgroups toward the air compartment. In the Langmuir monolayer experiment where this local reorganization has been for the first time observed by means of light scattering microscopy, water condensation on those hydrophilic lipid headgroups that have been exposed to the air—saturated with water vapor—leads to the formation of water droplets that facilitate visualization of the molecular event.

4.4. Energetics of surface structure reorganization

In the following we estimate the relevant energies pertinent to the proposed molecular scenario, concentrating on the initial and final states of the conjectured surface structure reorganization. The total energy that is liberated by the reorientation of one SP-C molecule, E_{reor}, may serve to invert a (yet unknown) number n of lipid molecules if this inversion process requires E_{inv} per lipid. While some of the energy, E_{diss}, may be dissipated in the subphase—e.g. due to reorganization of the hydration shell of immersed protein or lipid borne charges—an energy balance reads

$$E_{\mathrm{reor}} = nE_{\mathrm{inv}} + E_{\mathrm{diss}} \tag{1}$$

E_{reor} is the sum of three major contributions: the reduction, $\Delta E_{\mathrm{hphob}}$ (>0), of unfavorable contacts between the hydrophobic helix is the near-to-horizontal orientation; the energy, ΔE_{exp} (>0), liberated by re-expansion of the surrounding phospholipid film into the area yielded by the protein upon reorientation; and the energy, $\Delta E_{\mathrm{elstat}}$ (<0), needed to liberate the tilted helix from the position into which it is locked—presumably by electrostatic interactions, as argued in the previous section.

$\Delta E_{\mathrm{hphob}}$ is estimated from the change in contact area, ΔA, which the protein shares with the water subphase in the loaded-spring configuration and the surface tension, γ, between water and the valyl-rich hydrophobic helix surface

$$\Delta E_{\mathrm{hphob}} = -\gamma_{\mathrm{p}} \Delta A \tag{2}$$

If γ is taken to be ~ 50 mN/m (equivalent to the surface tension of water reduced by that of, e.g. pentane, ~ 15 mN/m, see [49]) and $\Delta A \sim 200$ Å^2, $\Delta E_{\mathrm{hphob}} \sim 10^{-19}$ J, equivalent to $\sim 25\ k_{\mathrm{B}}T$. ΔE_{exp} is the change in internal energy, ΔU, that the lipid monolayer undergoes upon expansion at constant T and constant π

$$\Delta E_{\mathrm{exp}} \approx \Delta U = -\pi \Delta A \tag{3}$$

in which the entropy change, ΔS, is given by the Maxwell relation,

$$\left.\frac{\Delta S}{\Delta A}\right|_T = \left.\frac{\partial \pi}{\partial T}\right|_A \tag{4}$$

which leads to

$$\Delta E_{\mathrm{exp}} = \left(-\pi + T\left(\frac{\partial \pi}{\partial T}\right)_A \right) \Delta A \tag{5}$$

If we assume that the area liberated per reoriented protein helix $\Delta A_{\mathrm{lib}} \sim 100$ Å^2 (smaller than the value used to estimate the hydrophobic contact, since the reoriented helix still uses area within the surface layer; this magnitude of ΔA_{lib} is, however, consistent with the experimentally observed area change upon compression of pure SP-C monolayers, see [44]) and use the experimentally determined value of

$$\left.\frac{\partial \pi}{\partial T}\right|_A \sim +1.5(\mathrm{mN/m\ K^{-1}})$$

for DPPC monolayers [50], we obtain $\Delta E_{\mathrm{exp}} \sim 4.4 \times 10^{-19}$ J, equivalent to $\sim 110\ k_{\mathrm{B}}T$.

The change in electrostatic energy, $\Delta E_{\mathrm{elstat}}$, conjectured to stabilize the hydrophobic helix in the loaded-spring configuration, is the most difficult to estimate. We note that in the initial state, $|E^{\mathrm{i}}_{\mathrm{elstat}}| \geqslant \Delta E_{\mathrm{hphob}}$, as the helix is stable in its loaded position at low surface pressure. A more definite estimate of $E^{\mathrm{i}}_{\mathrm{elstat}}$ is difficult since precise values for both the dielectric constants on both sides of the interface and the distance between charge and image charge are inaccessible. In the final orientation of the helix, normal to the interface, charge–image charge attraction leads to a reduction of $\Delta E_{\mathrm{elstat}} = E^{\mathrm{f}}_{\mathrm{elstat}} - E^{\mathrm{i}}_{\mathrm{elstat}}$ to a value lower than $\Delta E_{\mathrm{hphob}}$

$$E^{\mathrm{f}}_{\mathrm{elstat}} = \frac{q^2}{4\pi\varepsilon_0} \frac{1}{2d} \tag{6}$$

where q is the real charge and $2d \sim 70$ Å—twice the length of the hydrophobic helix—is the distance separating real and image charges. If $q = e$, the unit charge, $E^{i}_{elstat} \sim 3 \times 10^{-20}$ J, which leads to the estimate, $\Delta E_{elstat} \sim -7 \times 10^{-20}$ J, equivalent to $\sim -17\ k_B T$. With that, finally,

$$\Delta E_{reor} = \Delta E_{hphob} + \Delta E_{exp} + \Delta E_{elstat} \quad (7)$$

is estimated to be of the order of $\Delta E_{reor} = 120\ k_B T$, of which by far the major contribution comes from expansion of the lipid monolayer into the area voided by helix reorientation. Given that, the estimated for ΔE_{reor} is actually a lower limit since it does not account for area liberated by the inversion of lipid molecules from the monolayer film.

The inversion of phospholipids does not occur on an individual basis but is a collective reorientation of a number of molecules. This follows from the rather high value obtained for ΔE_{reor}. For an estimate of the energy, ΔE_{inv}, required for the inversion process per lipid molecule, one has thus to account for changes in the electrostatic energy—in a similar way as electrostatics entered the energetics of protein reorientation—and may in a first approximation neglect the loss of hydrophobic–hydrophobic contacts within the monolayer film. Let us assume that *all* inverted phospholipids belong to the charged PG species. If s (<0) is the location of the charge q with respect to the interface as long as the lipid molecule resides in the monolayer and d' is its distance (on the other side of the interfacial area) in the inverted state, we obtain

$$\Delta E_{inv} = \frac{q^2}{4\pi\varepsilon_0}\left(\frac{1}{2\varepsilon_r s} + \frac{1}{2d'}\right) \quad (8)$$

where ε_r is the permittivity of the aqueous surrounding of the hydrated headgroup; s is of the order of 5 Å [51,52] and $d' \sim d$. If we estimate $\varepsilon_r \sim 10$, we obtain $\Delta E_{inv} \sim 5 \times 10^{-20}$ J, equivalent to $\sim 12\ k_B T$. This result depends sensitively on ε_r and can only be regarded as a coarse estimate of the energy required to invert a charged phospholipid near the hydrophobic/hydrophilic interface. Nevertheless, it justifies a posteriori the neglect of changes in association energy between acyl chains due to the hydrophobic effect, since ~ 10 lipids are inverted in each protein reorientation event, and provides a first idea of how the nuclei of the much larger exclusion particles, which are presumably formed from these states, might look like. We emphasize that the rationale given above is just an *initial state/final state* assessment and that an energy barrier has to be surpassed during the course of SP-C reorientation as its terminal charge is drawn from the medium of higher polarization. An assessment of such details, however, seems out of reach as long as atomic-level properties of the interface—such as the local concentration of subphase-borne ions—remain unknown.

4.5. Putative role of SP-B in the inversion process

Our previously published results [25] as well as the research described in this current article implicate the hydrophobic surfactant protein SP-C as the primary causative agent for the appearance of the surface-associated 3D structures seen by dark-field scattered light microscopy. Other studies have also described a role for SP-C in the formation of 3D structures that adhere to the surface [19,45,46]. A model for the formation of a multibilayer phospholipid reservoir, stabilized by SP-C, has been proposed [19,47].

Much less information is available concerning the role of the other major hydrophobic surfactant protein, SP-B, in the formation of interfacial multilayer structures. Potentially, this is due to the fact that SP-B is the minor component in the full hydrophobic SP-B/C surfactant protein extract (molar ratio of 1:2 SP-B:SP-C). While the 78-residue SP-B protein contains four amphipathic helical segments [53], it also contains more polar and charged residues than does SP-C and is not as strongly membrane-associated as is the SP-C protein, thereby potentially limiting the efficiency of the SP-B protein in the formation of lipid–protein 3D particles. The major surfactant functions attributed to SP-B have been the creation of a reservoir for surfactant material and the promotion of the rapid re-insertion of phospholipids into the monolayer at the air/water interface [36,54].

Nevertheless, SP-B has been the subject of several recent optical studies that focused on the

role it plays in monolayer structural reorganization. Fluorescence and scanning probe microscopy were used to determine that SP-B induces a 2D–3D transformation of the fluid monolayer phase [22]. A separate optical microscopy study confirms the formation of 3D protein–lipid structures in monolayer films by SP-B, although these structures are much smaller (possibly only one molecule thick) and occur at a much reduced level from those formed from SP-C [20]. A truncated form of SP-B, SP-B_{1-25}, has been recently investigated in connection with phosphatidic acid, $C_{15}H_{31}COOH$, in surface monolayers. Starting from a molecular model that was derived from FT-IR and molecular simulations work [39], an X-ray scattering study revealed that SP-B_{1-25} is strongly associated with the surface monolayer [55,56]. How far these results may be transferred to the association of the native SP-B protein with lipid surfaces is unclear at the moment.

The presence of SP-B is not required in our model of the formation of 3D surface-associated lipid–protein particles by SP-C (Fig. 6). However, a comparison of the dark-field, scattered light images presented here (Fig. 5) and in our previously published results [25] suggests that while the presence of SP-B is not strictly necessary, it is nonetheless important for the efficient formation of these micrometer-sized 3D structures. A potential explanation of the role of SP-B is that of a low-cooperativity nucleation site for the SP-C reorientation process. As argued above, the energetics of the formation of the observed surface-associated 3D particles must be a highly cooperative process. SP-B, however, appears to bind relatively few lipids and remains at or near the interface during monolayer compression. In this view, SP-B acts as the nucleation site or catalyst for the formation of the larger, i.e. micrometer-sized, 3D lipid–protein domains that develop in a highly cooperative process of SP-C reorientation.

5. Conclusions

We have investigated the functional role of SP-C in surface phospholipid monolayers using fluorescent microscopy in combination with a modified dark-field, scattered light microscopy. The results presented here, when compared with our previous results [25], obtained using the entire fraction of hydrophobic surfactant protein (SP-B/C), lead to the following conclusions concerning the functional role of SP-C.

(1) The individual SP-C protein does not possess the same ability to alter monolayer morphology as does the full hydrophobic surfactant protein fraction. In addition, SP-C by itself does not catalyze the formation of 3D, surface-associated, particles at physiologically relevant protein concentrations ($\sim$1 wt.%). However, at somewhat higher protein concentrations ($\sim$10 wt.%), the effect of the individual SP-C protein does begin to resemble that of the full SP-B/C hydrophobic surfactant protein mixture. In particular, we have utilized a synthetic SP-C molecule derivatized with a fluorescent probe to compare the fluorescence intensity distributions from lipid and protein dyes. In nearly simultaneous image acquisitions, we were able to show that SP-C is preferentially associated with disordered monolayer phases. In addition, the presence of the labeled SP-C at these higher (10 wt.%) concentrations results in a monolayer morphology nearly identical to that of the SP-B/C protein at low (1 wt.%) concentrations. The labeled SP-C accelerates the dissolution of condensed phase domains and the formation of a new, lower order phase in the monolayer that is morphologically similar to what we have observed with the entire SP-B/C fraction.

(2) The fluorescently labeled SP-C also catalyzes the formation of micrometer-sized, surface-associated, 3D particles at the interface, as visualized using scattered light dark-field microscopy with grazing incidence laser illumination. Using sequential fluorescence and scattered light microscopy, it is easily shown that the 3D particles are associated exclusively with the presence of the SP-C protein in the fluid monolayer phase.

(3) Using our optical microscopy results in conjunction with other literature studies, we have developed a model that describes a mechanism by which SP-C could catalyze the formation of the observed 3D, surface-associated particles. In this model, SP-C acts analogously to a molecular machine, or loaded spring, in which the stored

energy of its hydrophobic rigid alpha helix is released upon reorientation around its flexible hydrophilic N-terminus, which is anchored at the A/W interface. This helical reorientation cooperatively causes an inversion of neighboring phospholipid molecules to form a locally confined bilayer structure. This model is supported by a simple energetic argument that shows that the major contributing factor to the formation of the 3D particles is the energy liberated by re-expansion of the surrounding phospholipid film into the area vacated by the SP-C protein as it re-orients away from the interface (estimated as $\sim 110\ k_B T$). These localized bilayers may act as a nucleus for further growth or a controlled collapse as described by other groups.

Acknowledgments

This work was supported by the US Public Health Service through NIH grants GM40117 (RAD), TW00877 (RAD), RR13982 (JEB) and by the DFG through the Sonderforschungsbereich 294, project no. G3 (ML). The work in Leipzig has also been supported by the Fonds der Chemischen Industrie, Frankfurt/M. P.K. has been supported by a post-doctoral grant through the US NIH.

References

[1] S. Schürch, J. Goerke, J.A. Clements, Direct determination of volume and time-dependence of alveolar surface tension in excised lung, Proc. Natl. Acad. Sci. USA 75 (1978) 3417–3421.

[2] E.M. Scarpelli, Surfactants and the Lining of the Lung, The Johns Hopkins University Press, Baltimore, 1988.

[3] M.E. Avery, J. Mead, Surface properties in relation to atelectasis and hyaline membrane disease, Am. J. Dis. Child. 97 (1959) 517–523.

[4] U. Pison, W. Seeger, R. Buchhorn, et al., Surfactant abnormalities in patients with respiratory failure after multiple trauma, Am. Rev. Respir. Dis. 140 (1989) 1033–1039.

[5] S.B. Hall, Z. Wang, R.H. Notter, Separation of subfractions of the hydrophobic components of calf lung surfactant, J. Lipid Res. 35 (1994) 1386–1394.

[6] M.C. Kahn, G.J. Anderson, W.R. Anyan, S.B. Hall, Phosphatiylcholine molecular species of calf lung surfactant, Am. J. Physiol. 269 (1995) L567–L573.

[7] J.E. Baatz, Y. Zou, J.T. Cox, Z. Wang, R.H. Notter, High yield purification of lung surfactant proteins SP-B and SP-C and the effects on surface activity, Protein Express. Purificat. 23 (2001) 180–190.

[8] S. Schürch, H. Bachofen, Surfactant therapy for lung diseases, in: B. Robertson, H.W. Tauesch (Eds.), Biophysical Aspects in the Design of a Therapeutic Surfactant, Marcel Dekker, New York, 1995, pp. 3–32.

[9] S. Hawgood, K. Schiffer, Structures and properties of the surfactant-associated proteins, Annu. Rev. Physiol. 53 (1991) 375–394.

[10] J. Johansson, T. Curstedt, B. Robertson, The proteins of the surfactant system, Eur. Respir. J. 7 (1994) 372–391.

[11] S. Hawgood, F.R. Poulain, Functions of the surfactant proteins: a perspective, Pediatr. Pulmonol. 19 (1995) 99–104.

[12] M.A. Oosterlaken-Dijksterhuis, H.P. Haagsman, L.M.G.v. Golde, R.A. Demel, Characterization of lipid insertion into monomolecular layers mediated by lung surfactant proteins SP-B and SP-C, Biochemistry 30 (1991) 10965–10971.

[13] V. Schram, S.B. Hall, Thermodynamic effects of the hydrophobic surfactant proteins on the early adsorption of pulmonary surfactant, Biophys. J. 81 (2001) 1536–1546.

[14] M.A. Oosterlaken-Dijksterhuis, H.P. Haagsman, L.M.G.v. Golde, R.A. Demel, Interaction of lipid vesicles with monomolecular layers containing lung surfactant proteins SP-B or SP-C, Biochemistry 30 (1991) 8276–8281.

[15] J. Perez-Gil, J. Tucker, G. Simatos, K. Keough, Interfacial adsorption of simple lipid mixtures combined with hydrophobic surfactant protein from pig lung, Biochem. Cell Biol. 70 (1992) 332–338.

[16] Z. Wang, S.B. Hall, R.H. Notter, Dynamic surface activity of films of lung surfactant phospholipids, hydrophobic proteins, and neutral lipids, J. Lipid Res. 36 (1995) 1283–1293.

[17] K. Nag, K.M.W. Keough, Epifluorescence microscopic studies of monolayers containing mixtures of dioleoyl- and dipalmitoylphosphatidylcholines, Biophys. J. 65 (1993) 1019–1026.

[18] K. Nag, N.H. Rich, K.M.W. Keough, Interaction between dipalmitoylphosphatidylglycerol and phosphatidylcholine and calcium, Thin Solid Films 244 (1994) 841–844.

[19] A. Kramer, A. Wintergalen, M. Sieber, H.J. Galla, M. Amrein, R. Guckenberger, Distribution of the surfactant-associated protein C within a lung surfactant model film investigated by near-field optical microscopy, Biophys. J. 78 (2000) 458–465.

[20] S. Krol, M. Ross, M. Sieber, S. Kunneke, H.J. Galla, A. Janshoff, Formation of three-dimensional protein–lipid aggregates in monolayer films induced by surfactant protein B, Biophys. J. 79 (2000) 904–918.

[21] J. Ding, D.Y. Takamoto, A. von Nahmen, et al., Effects of lung surfactant proteins, SP-B and SP-C, and palmitic

acid on monolayer stability, Biophys. J. 80 (2001) 2262–2272.
[22] D.Y. Takamoto, M.M. Lipp, A. von Nahmen, K.Y.C. Lee, A. Waring, J.A. Zasadzinski, Interaction of lung surfactant proteins with anioinic phospholipids, Biophys. J. 81 (2001) 153–169.
[23] K. Nag, J. Perez-Gil, A. Cruz, K.M.W. Keough, Fluorescently labeled pulmonary surfactant protein C in spread phospholipid monolayers, Biophys. J. 71 (1996) 246–256.
[24] K. Nag, S.G. Taneva, J. Perez-Gil, A. Cruz, K.M.W. Keough, Combinations of fluorescently labeled pulmonary surfactant proteins SP-B and SP-C in phospholipid films, Biophys. J. 72 (1997) 2638–2650.
[25] P. Krüger, M. Schalke, Z. Wang, R.H. Notter, R.A. Dluhy, M. Lösche, Effect of hydrophobic surfactant peptides SP-B and SP-C on binary phospholipid monolayers. I. Fluorescence and dark-field microscopy, Biophys. J. 77 (1999) 903–914.
[26] R.B. Merrifield, L.D. Vizioli, H.G. Boman, Synthesis of the antibacterial peptide cecropin A (1-33), Biochemistry 21 (1982) 5020–5031.
[27] Z. Wang, O. Gurel, J.E. Baatz, R.H. Notter, Differential activity and lack of synergy of lung surfactant proteins SP-B and SP-C in interactions with phospholipids, J. Lipid Res. 37 (1996) 1749–1760.
[28] A.D. Horowitz, B. Moussavian, E.D. Han, J.E. Baatz, J.A. Whitsett, Distinct effects of SP-A and SP-B on endocytosis of SP-C by pulmonary epithelial cells, Am. J. Physiol. 273 (1997) L159–L171.
[29] G.N. Enhorning, Pulsating bubble technique for evaluating pulmonary surfactant, J. Appl. Physiol.: Respir. Environ. Excer. Physiol. 43 (1977) 198–203.
[30] S.B. Hall, M.S. Bermel, Y.T. Ko, H.J. Palmer, G.N. Enhorning, R.H. Notter, Approximations in the measurement of surface tension on the oscillating bubble surfactometer, J. Appl. Physiol. 75 (1993) 468–477.
[31] Y.S. Shin, Spectrophotometric ultramicrodetermination of inorganic phosphorus and lipid phosphorus in serum, Anal. Chem. 34 (1962) 1164–1166.
[32] J. Johansson, T. Szyperski, T. Curstedt, K. Wüthrich, The NMR structure of the pulmonary surfactant-associated polypeptide SP-C in an apolar solvent contains a valyl-rich α-helix, Biochemistry 33 (1994) 6015–6023.
[33] E. Goormaghtigh, V. Cabiaux, J.-M. Ruysschaert, Physiochemical methods in the study of biomembranes, in: H.J. Hilderson, G.B. Ralston (Eds.), Determination of Soluble and Membrane Protein Structure by Fourier Transform Infrared Spectroscopy. I. Assignments and Model Compounds, vol. 23, Plenum Press, New York, 1994, pp. 329–362.
[34] C.W. McConlogue, T.K. Vanderlick, A close look at domain formation in DPPC monolayers, Langmuir 13 (1997) 7158–7164.
[35] R.A. Dluhy, K.E. Reilly, R.D. Hunt, M.L. Mitchell, A.J. Mautone, R. Mendelsohn, Infrared spectroscopic investigations of pulmonary surfactant. Surface film transitions at the air–water interface and bulk phase thermotropism, Biophys. J. 56 (1989) 1173–1181.
[36] J.E. Baatz, B. Elledge, J.A. Whitsett, Surfactant protein SP-B induces ordering at the surface of model membrane bilayers, Biochemistry 29 (1990) 6714–6720.
[37] B. Pastrana-Rios, S. Taneva, K.M.W. Keough, A.J. Mautone, R. Mendelsohn, External reflection absorption infrared spectroscopy study of lung surfactant proteins SP-B and SP-C in phospholipid monolayers at the air/water interface, Biophys. J. 69 (1995) 2531–2540.
[38] A. Gericke, C.R. Flach, R. Mendelsohn, Structure and orientation of lung surfactant SP-C and L-α-dipalmitoylphosphatidylcholine in aqueous monolayers, Biophys. J. 73 (1997) 492–499.
[39] L.M. Gordon, K.Y.C. Lee, M.M. Lipp, et al., Conformational mapping of the N-terminal segment of surfactant protein B in lipid using C-13-enhanced Fourier transform infrared spectroscopy, J. Peptide Res. 55 (2000) 330–347.
[40] M.M. Lipp, K.Y.C. Lee, J.A. Zasadzinski, A.J. Waring, Phase and morphology changes in lipid monolayers induced by SP-B protein and its amino-terminal peptide, Science 273 (1996) 1196–1199.
[41] M.M. Lipp, K.Y.C. Lee, A. Waring, J. Zasadzinski, Fluorescence, polarized fluorescence and Brewster angle microscopy of palmitic acid and lung surfactant protein B monolayers, Biophys. J. 72 (1997) 2783–2790.
[42] J. Perez-Gil, K. Nag, S. Taneva, K. Keough, Pulmonary surfactant protein SP-C causes packing rearrangements of dipalmitoylphosphatidylcholine in spread monolayers, Biophys. J. 63 (1992) 197–204.
[43] J.M. Brockman, Z. Wang, R.H. Notter, R.A. Dluhy, Effect of hydrophobic surfactant proteins SP-B and SP-C on binary phospholipid monolayers. II. Infrared external reflectance–absorption spectroscopy, Biophys. J., submitted for publication.
[44] A. Post, A. von Nahmen, M. Schmitt, et al., Pulmonary surfactant protein C containing lipid films at the air–water interface as a model for the surface of lung alveoli, Mol. Membr. Biol. 12 (1995) 93–99.
[45] M. Amrein, A. von Nahmen, M. Sieber, A scanning force and fluorescence light microscopy study of the structure and function of a model pulmonary surfactant, Biophys. J. 26 (1997) 349–357.
[46] A. von Nahmen, M. Schenk, M. Sieber, M. Amrein, The structure of a model pulmonary surfactant as revealed by scanning force microscopy, Biophys. J. 72 (1997) 463–469.
[47] H.J. Galla, N. Bourdos, A. von Nahmen, M. Amrein, M. Sieber, The role of pulmonary surfactant protein C during the breathing cycle, Thin Solid Films 329 (1998) 632–635.
[48] N. Bourdos, F. Kollmer, A. Benninghoven, M. Ross, M. Sieber, H.J. Galla, Analysis of lung surfactant model systems with time-of-flight secondary ion mass spectrometry, Biophys. J. 79 (2000) 357–369.

[49] D.R. Lide, CRC Handbook of Chemistry and Physics, CRC Press, Boca Raton, 2000.
[50] O. Albrecht, H. Gruler, E. Sackmann, Polymorphism of phospholipid monolayers, J. Physique (France) 39 (1978) 301–313.
[51] M. Schalke, P. Krüger, M. Weygand, M. Lösche, Submolecular organization of DMPA in surface monolayers: beyond the two-layer model, Biochim. Biophys. Acta 1464 (2000) 113–126.
[52] P. Krüger, M. Lösche, Molecular chirality and the domain shapes in lipid monolayers on aqueous surfaces, Phys. Rev. E 62 (2000) 7031–7043.
[53] S. Hawgood, M. Derrick, P. Poulain, Structure and properties of surfactant protein B, Biochim. Biophys. Acta 1408 (1998) 150–160.
[54] S.-H. Yu, F. Possmayer, Effect of pulmonary surfactant protein B (SP-B) and calcium on phospholipid adsorption and squeeze-out of phosphatidylglycerol from binary phospholipid monolayers containing dipalmitoylphosphatidylcholine, Biochim. Biophys. Acta 1126 (1992) 26–34.
[55] K.Y.C. Lee, J. Majewski, T.L. Kuhl, et al., The incorporation of lung surfactant specific protein SP-B into lipid monolayers at the air–fluid interface: a grazing incidence X-ray diffraction study, Mat. Res. Soc. Symp. Proc. 590 (2000) 177–182.
[56] K.Y.C. Lee, J. Majewski, T.L. Kuhl, et al., Synchrotron X-ray study of lung surfactant-specific protein SP-B in lipid monolayers, Biophys. J. 81 (2001) 572–585.
[57] D.A. Cadenhead, F. Müller-Landau, B.M.J. Kellner, Ordering in two dimensions, in: S.K. Sinha (Ed.), Phase Transitions in Insoluble One and Two-Component Films at the Air/Water Interface, Elsevier, Amsterdam, 1980, pp. 73–81.